https://doi.org/10.5194/egusphere-2026-2304
Preprint. Discussion started: 20 May 2026

Impact of ROMEX Radio Occultation Bending Angle Assimilation on Mesoscale Weather Prediction over the Indian Region

Randhir Singh[1], Satya P. Ojha[1], Kudilil Faisal Muhammed[1], and Richard Anthes[2]

[1]Space Applications Centre, Indian Space Research Organisation (ISRO), Ahmedabad-380015, India
[2]University Corporation for Atmospheric Research (UCAR), Boulder, CO 80301, USA

Correspondence to: Randhir Singh (randhir_h@yahoo.com)

Abstract. Data assimilation experiments were conducted for September 2022 at 9-km horizontal resolution using a cyclic three-dimensional variational (3D-Var) assimilation system to assess the impact of a large number of Global Navigation Satellite System (GNSS) radio occultation (RO) bending angle data on mesoscale weather prediction over the Indian region. To enable this, a bending angle observation operator was implemented within the WRF (Weather Research and Forecasting) data assimilation system.

Two experiments were performed: a control experiment (CNTL), in which only conventional observations were assimilated, and a second experiment (RMX-BA), in which RO bending angle observations from the Radio Occultation Modelling Experiment (ROMEX) were assimilated along with conventional data. A 6-h assimilation cycle was performed throughout September 2022. From the 00 and 12 UTC analyses, 72-h forecasts were generated daily, resulting in approximately 60 forecast cases.

Forecasts from both experiments were verified against ERA5 reanalysis for water vapor, temperature, and wind, while rainfall forecasts were compared against Integrated Multi-satellite Retrievals for GPM (IMERG) rainfall estimates. The results show that assimilating RO data improves both the analyses and forecasts of specific humidity, temperature, wind, and rainfall compared to the CNTL experiment. The rainfall forecast skill improved significantly, mainly due to more accurate water vapor in the model's initial conditions. The moist total energy norm (TE), which accounts for forecast errors in water vapor, wind, temperature, and pressure, was reduced by about 20% at the analysis time and by approximately 8.5% in the 72-h forecast.

Overall, the study demonstrated that assimilation of RO bending angle data significantly improved mesoscale weather forecasts over the Indian region.

1 Introduction

Satellite observations play a critical role in improving the initial conditions of mesoscale numerical weather prediction (NWP), particularly over regions such as the Indian subcontinent and the surrounding oceanic areas where conventional observations are sparse. High-resolution forecasts are especially sensitive to errors in thermodynamic variables, including temperature and water vapor, which strongly influence convective instability and precipitation processes during the monsoon season. In the absence of dense in situ measurements, satellite observations play a crucial role in constraining the atmospheric state over

https://doi.org/10.5194/egusphere-2026-2304
Preprint. Discussion started: 20 May 2026

data-sparse regions and have become one of the most important data sources for NWP, significantly improving forecast skill when assimilated into operational models (Geer et al., 2018).

Among the various satellite observing systems currently available, GNSS RO has emerged as one of the most impactful sources of high-vertical-resolution atmospheric information in NWP (Cardinali and Healy, 2014; Anthes et al. 2024) with long-term stability and minimal bias (Kursinski et al., 1997; Anthes et al., 2000; Anthes et al., 2008). RO observations are obtained by measuring the phase delay and bending of GNSS signals as they propagate through Earth's atmosphere, from which atmospheric refractivity profiles can be derived. These refractivity profiles are directly related to temperature, pressure, and water vapour through well-established physical relationships.

Early RO missions such as CHAMP, GRACE, and FORMOSAT-3/COSMIC demonstrated the utility of RO observations in improving large-scale atmospheric analyses and NWP forecast skill (Anthes et al., 2008). Subsequent operational RO missions, including the MetOp series carrying the GRAS (GNSS Receiver for Atmospheric Sounding) instrument and the COSMIC-2 (FORMOSAT-7) constellation launched in 2019, have significantly increased the availability of RO observations for operational weather forecasting (Schreiner et al., 2020). The COSMIC-2 mission alone consists of six low-Earth-orbit satellites capable of providing more than 5000 high-quality atmospheric profiles per day for NWP applications.

Assimilation of RO observations in global NWP systems has been shown to improve temperature analyses in the upper troposphere and lower stratosphere and enhance forecast skill in both medium-range and short-range prediction (Healy and Thepaut, 2006; Cucurull et al., 2007; Poli et al., 2010; Cardinali and Healy, 2014; Bowler, 2020; Hong et al., 2023; Anthes et al., 2024). Many studies have also demonstrated that assimilation of RO observations in regional NWP models improves mid-tropospheric water vapor fields and reduces forecast errors, leading to enhanced precipitation and improved tropical cyclone forecasts (Chen et al., 2009; Huang et al. 2010;Liu and Xue, 2014; Miller et al., 2023 and 2026; Johnston et al., 2025; Xuan et al. 2025). Lonitz et al. (2025) showed that RO observations are useful for improving sub seasonal forecasts, with their positive impact remaining evident up to 3–4 weeks. Purwar et al. (2025) demonstrated the positive impact of both ground-based and space-based GNSS observations on extreme rainfall events over Karnataka, India.

Traditionally, refractivity profiles derived from RO measurements have been assimilated into limited-area NWP systems. However, refractivity retrieval involves inversion procedures that introduce background-dependent assumptions and smoothing effects. In contrast, bending angle observations are closer to the original occultation measurements and therefore retain higher information content (Healy et al., 2007; Healy and Thepaut, 2006; Healy, 2001; Cucurull et al., 2007, 2013). Several studies have demonstrated that assimilation of bending angles can provide improved thermodynamic analyses compared to refractivity assimilation, particularly in data-sparse regions. Therefore, most operational centers assimilate bending angles rather than refractivity.

In recent years, the availability of RO observations has increased substantially due to the emergence of commercial missions. Private satellite constellations operated by companies such as Spire Global and PlanetiQ provide large volumes of RO observations using low-cost CubeSat platforms. The increasing number of commercial RO satellites has led to a significant growth in the global availability of atmospheric profiles, and today commercial and government RO constellations can collectively provide more than 20,000 atmospheric soundings per day for weather forecasting applications.

Furthermore, observations disseminated through the Global Telecommunication System (GTS) for operational NWP systems typically represent only a subset of the available RO observations. The Radio Occultation Modeling Experiment (ROMEX) provides a significantly higher density of RO profiles (Anthes et al., 2024) for a three-month period (September-November 2022). ROMEX is an international collaborative initiative aimed at assessing the scientific and operational benefits of substantially increasing the number of RO observations for NWP and climate applications well beyond current operational availability. During ROMEX, RO observations from both government-funded missions and commercial satellite constellations were collected, processed, archived, and made available for research and data assimilation experiments. This combined dataset consisted of approximately 30,000–35,000 RO profiles per day, nearly three times the number of profiles typically available in operational NWP systems during the same period. Anthes et al. (2025) evaluated the biases and uncertainties of ROMEX data and confirmed the quality and compatibility of these high-volume observations for NWP assimilation.

Several recent global assimilation studies within the framework of ROMEX have demonstrated that increasing the number of assimilated RO profiles leads to improved forecast skill across key atmospheric variables such as temperature, humidity, geopotential height, and wind speed. For example, Zhang et al. (2025) showed that assimilating larger numbers of RO observations in the NOAA Global Forecast System (GFS) significantly reduces forecast errors and enhances verification metrics against both observations and analyses compared to experiments with fewer RO profiles, with benefits persisting up to five days of forecast. Other studies have shown that assimilating ROMEX observations improves forecasts of tropical cyclones (Johnston et al., 2025) and atmospheric rivers (Lin et al. 2026). These studies confirm that forecast improvements generally scale with the number of RO profiles assimilated, with little evidence of saturation even at densities (35,000 profiles per day) much higher than typical operational levels.

The objective of the present study is to evaluate the impact of assimilating ROMEX bending angle observations on mesoscale NWP over the Indian region. Data assimilation experiments were conducted using the WRF model and its data assimilation system during the end of the summer monsoon period, September 2022. This study is the first to assimilate ROMEX bending angle observations into the WRF model to evaluate their impact on regional weather prediction over the Indian region.

2 Model configuration and data assimilation system

2.1 WRF model

The Advanced Research Weather Research and Forecasting (WRF-ARW) model was used to conduct the numerical experiments (Skamarock et al., 2019). The model domain covers the Indian region and adjoining oceans with a horizontal grid spacing of 9 km and consists of 600 × 600 grid points, with the domain centre located at 20° N, 80° E (Figure 1).

https://doi.org/10.5194/egusphere-2026-2304
Preprint. Discussion started: 20 May 2026

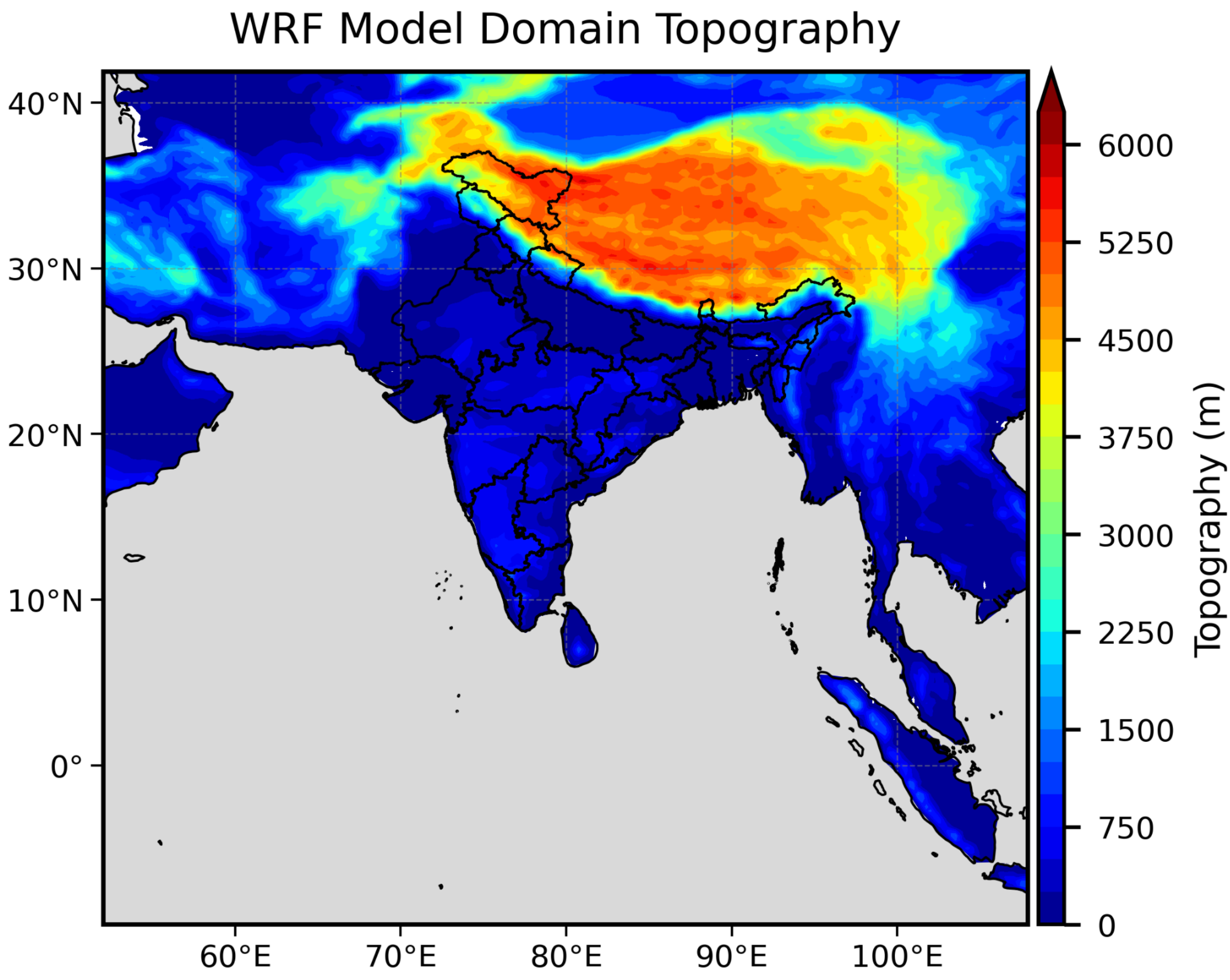

Figure 1. WRF model domain and topography used in this study. The domain covers the Indian region and adjoining oceanic areas at 9 km horizontal resolution.

The model configuration includes 41 vertical levels extending from the surface to a model-top pressure of 10 hPa. The physical parameterization schemes employed include the WSM6 graupel microphysics scheme, the Kain–Fritsch (new Eta) cumulus parameterization, the Yonsei University (YSU) planetary boundary layer scheme, the Noah land surface model, and the Dudhia shortwave and longwave radiation schemes.

2.2 WRF data assimilation (WRF-DA)

Data assimilation was performed using the WRF-DA system employing the three-dimensional variational (3D-Var) technique (Barker et al., 2012). The background error covariance matrix was generated using the NMC method (Parrish and Derber, 1992), based on differences between 48-h and 24-h WRF forecasts. Bending angle observations from ROMEX were assimilated using the WRF-DA radio occultation forward operator, which computes model-equivalent bending angles. By default, WRF-DA can directly assimilate only refractivity observations, and a bending angle observation operator is not available in the standard WRF-DA system. Since ROMEX provides bending angle measurements rather than refractivity, a bending angle observation operator was integrated into the WRF-DA system for this study. The bending angle operator formulation proposed by the ROM SAF was adopted and implemented within the WRF-DA system. Details of the bending angle observation operator implemented in WRF-DA are described in subsection 2.4.

2.3 Experimental design

First, a control (CNTL) experiment was performed in which only conventional observations were assimilated, including radiosonde, SYNOP, METAR, ship and buoy reports, satellite-derived winds (atmospheric motion vectors, AMVs), and scatterometer-derived surface winds. In the second experiment (RMX-DA), conventional observations were assimilated together with bending angle observations from ROMEX. The only difference between the two experiments was the use of RO bending angle observations. To better isolate and assess the maximum potential of ROMEX data, radiance observations were intentionally excluded from the assimilation in this study.

All observations assimilated in the model underwent a quality-control procedure in which observations differing from the background by more than five times the specified observation error were rejected. This is the default quality-control procedure implemented in WRF-DA. The same criterion was applied to RO observations. The observation errors for RO data were specified based on the GFS (GSI data assimilation) operational configuration (Cucurull et al., 2013; Kleist et al., 2009), whereas the errors for conventional observations were taken from the datasets themselves. It should be noted that in the operational GFS configuration, RO assimilation is implemented conservatively with relatively larger observation error assumptions. In this study, the same quality control procedures and error specifications as those used in GFS were adopted, and no additional experiments with alternative quality control criteria or error settings were conducted.

A 6-hourly data assimilation cycling was performed in which analyses were produced at synoptic hours (00:00, 06:00, 12:00, and 18:00 UTC) using an assimilation window of ± 3 hours. The first assimilation was performed at 00:00 UTC on 1 September 2022, using a 6-h WRF forecast initialized from the ERA5 reanalysis (Hersbach et al. 2020) at 18:00 UTC on 31 August 2022. A total of 120 analyses were produced over the entire month. The 6-hourly ERA5 reanalysis was used to provide the model boundary conditions. A 72-h forecast was generated daily at 00:00 UTC and 12:00 UTC throughout September 2022. All experiments were conducted at 9-km resolution over identical periods and with the same forecast lengths to isolate the impact of RO assimilation. Figure 2 shows the data assimilation framework adopted in this study.

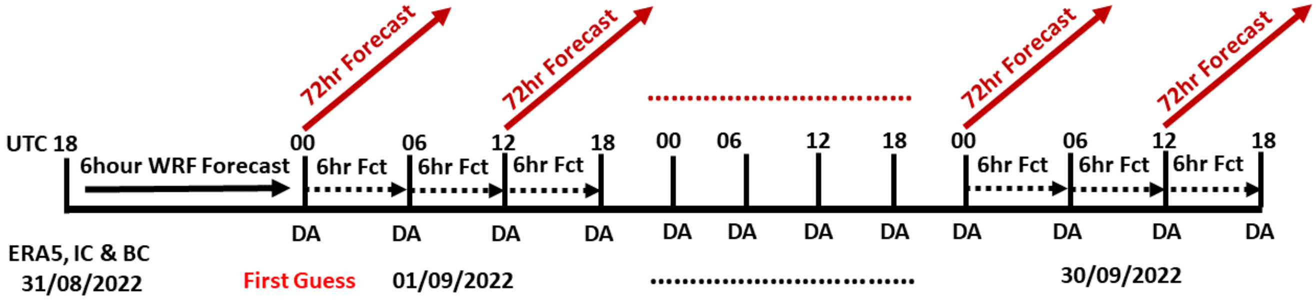

Figure 2. Cycling data assimilation framework and forecast design used in this study. Analyses were produced every 6 h and 72 h forecasts were launched from the 00:00 and 12:00 UTC analyses.

2.4 RO bending-angle forward observation operator

RO refractivity profiles assimilated in NWP systems are typically obtained through an Abel inversion of bending angle measurements. However, refractivity retrieval involves smoothing and background-dependent assumptions that can introduce representativeness errors and reduce the effective information content of the observations, as discussed by Healy and Thepaut (2006). In contrast, bending angle observations represent a more direct measurement derived from the phase delay of GNSS signals as they traverse the atmosphere. Assimilation of bending angle measurements therefore enables the use of higher-information-content observations while avoiding the additional assumptions introduced during refractivity retrieval.

In most operational NWP systems, a 1D forward operator is used for RO bending angle assimilation because it is computationally efficient and simple to implement. The 1D operator assumes that the atmosphere is horizontally uniform around the tangent point (spherically symmetric) and computes bending angles from a single vertical refractivity profile using the Abel transform. However, this assumption ignores horizontal gradients and can introduce errors in regions with strong horizontal variability, such as fronts, convection, monsoon systems, and tropical cyclones (e.g., Kursinski et al., 1997; Healy, 2001). Therefore, in this study we use a 2D forward operator, which accounts for horizontal variability in the vertical plane of the occultation and performs ray tracing through a two-dimensional refractivity field. This approach provides a more realistic representation of the atmosphere and helps reduce forward-model errors, especially in dynamically active mesoscale regions (e.g., Zou et al., 1999;Syndergaard, 2012). Although the 2D operator is computationally more expensive, it is better suited for studies focusing on mesoscale processes and regions with strong horizontal gradients.

The two-dimensional (2D) bending angle forward operator was integrated into the WRF-DA system, enabling the direct assimilation of RO bending angle observations. The 2D bending angle forward operator (FWD) used in this study was originally developed at ECMWF (Eyre, 1994; Healy et al., 2007). It includes the forward (FWD), tangent linear (TL), and adjoint (AD) operators required for variational data assimilation. This operator is implemented within the Radio Occultation Processing Package (ROPP) (Culverwell et al., 2015), which is maintained under the EUMETSAT Radio Occultation Meteorology Satellite

https://doi.org/10.5194/egusphere-2026-2304
Preprint. Discussion started: 20 May 2026

Application Facility (ROM SAF). A detailed technical description of the operator is provided in the official ROPP user guide (ROM SAF, 2021).

In brief, the 2D operator requires meteorological variables defined along the occultation plane for each ray path (Figure 3).

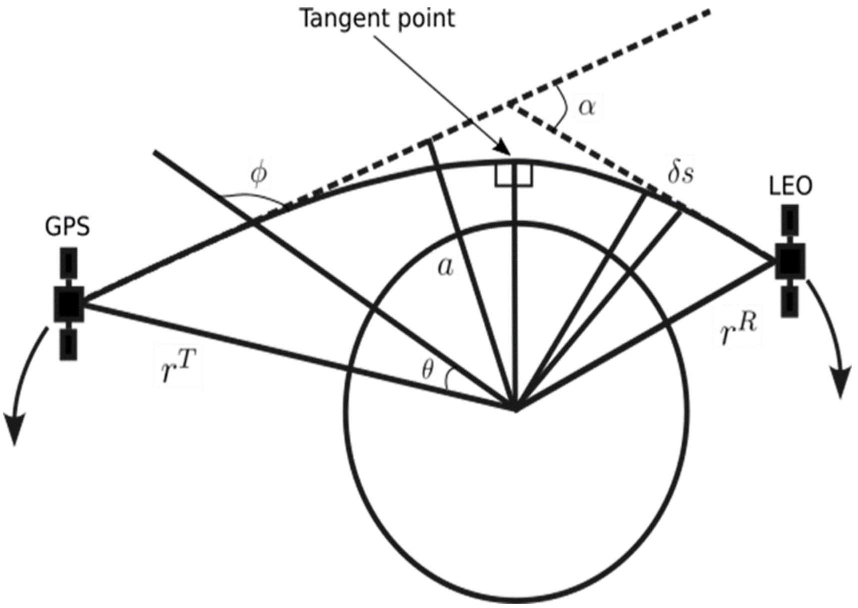

Figure 3. Geometry of GNSS radio occultation and the occultation plane used by the two-dimensional bending-angle forward operator.

The occultation plane is constructed using 31 vertical profiles extracted at equally spaced locations, with an angular separation of dθ = 6.27844 $\times$ 10^{-3} radians, corresponding to a horizontal spacing of approximately 40 km at the Earth's surface. These configuration settings follow Healy et al. (2007). The parameters required to define the occultation plane—such as geolocation, impact parameter, and azimuth angle at the tangent point—are directly obtained from the observation files.

Refractivity (N) at model levels is calculated from vertical profiles of air pressure (P), water vapor pressure (e), and temperature (T) using the two-term empirical formula proposed by Smith and Weintraub (1953).

$$N = 77.6\frac{P}{T} + 3.73 \times 10^5 \frac{e}{T^2} \quad (1)$$

The calculation is performed without considering the effects of non-ideal gas compressibility (Aparicio et al., 2009). The refractive-index radius product, , is pre-computed at the model levels and used as a two-dimensional input field for the ray tracer. We assume a single occultation point for each bending angle within a profile; therefore, tangent point drift is neglected. The bending angle is calculated by numerically solving the differential equations that describe the ray path in circular polar (r, θ) coordinates (Rodgers, 2000).

$$\frac{\mathrm{d}r}{\mathrm{d}s} = \cos\phi \tag{2}$$

$$\frac{\mathrm{d}\theta}{\mathrm{d}s} = \frac{\sin\phi}{r} \tag{3}$$

$$\frac{\mathrm{d}\phi}{\mathrm{d}s} = -\frac{1}{n}\frac{\mathrm{d}n}{\mathrm{d}r}\sin\phi \tag{4}$$

Here, s represents the distance along the ray path, n is the atmospheric refractive index at a given point along the ray, and ϕ is the angle between the local radius vector and the tangent to the ray path. These equations are solved using a fourth-order Runge–Kutta method with an adaptive step size. It is assumed that refractivity varies exponentially with height between model levels. The analytical formula proposed by Healy and Thepaut (2006) was used to calculate the bending angle above the model top using a 1D approach. The model variables used in this formulation are extrapolated using variables at the top of the model.

3 Assimilation results

3.1 Assimilated GNSS-RO observations

Figure 4 shows the temporal variation in the number of RO profiles assimilated in RMX-BA experiment at each 6-h assimilation cycle throughout the study period.

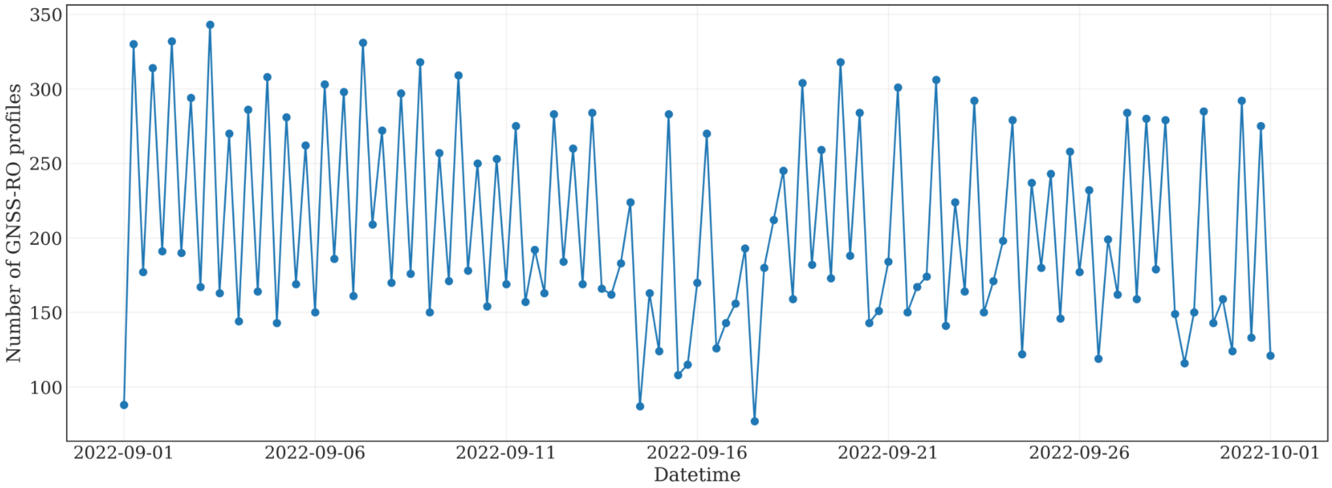

Figure 4. Temporal variation in the number of GNSS-RO profiles assimilated in the RMX-BA experiment for each 6 h analysis cycle during September 2022.

The number of assimilated profiles ranges from 90 to 345. Figure 5 presents the spatial distribution of assimilated profiles on a 5° × 5° grid for each experiment, accumulated over the entire period.

https://doi.org/10.5194/egusphere-2026-2304
Preprint. Discussion started: 20 May 2026

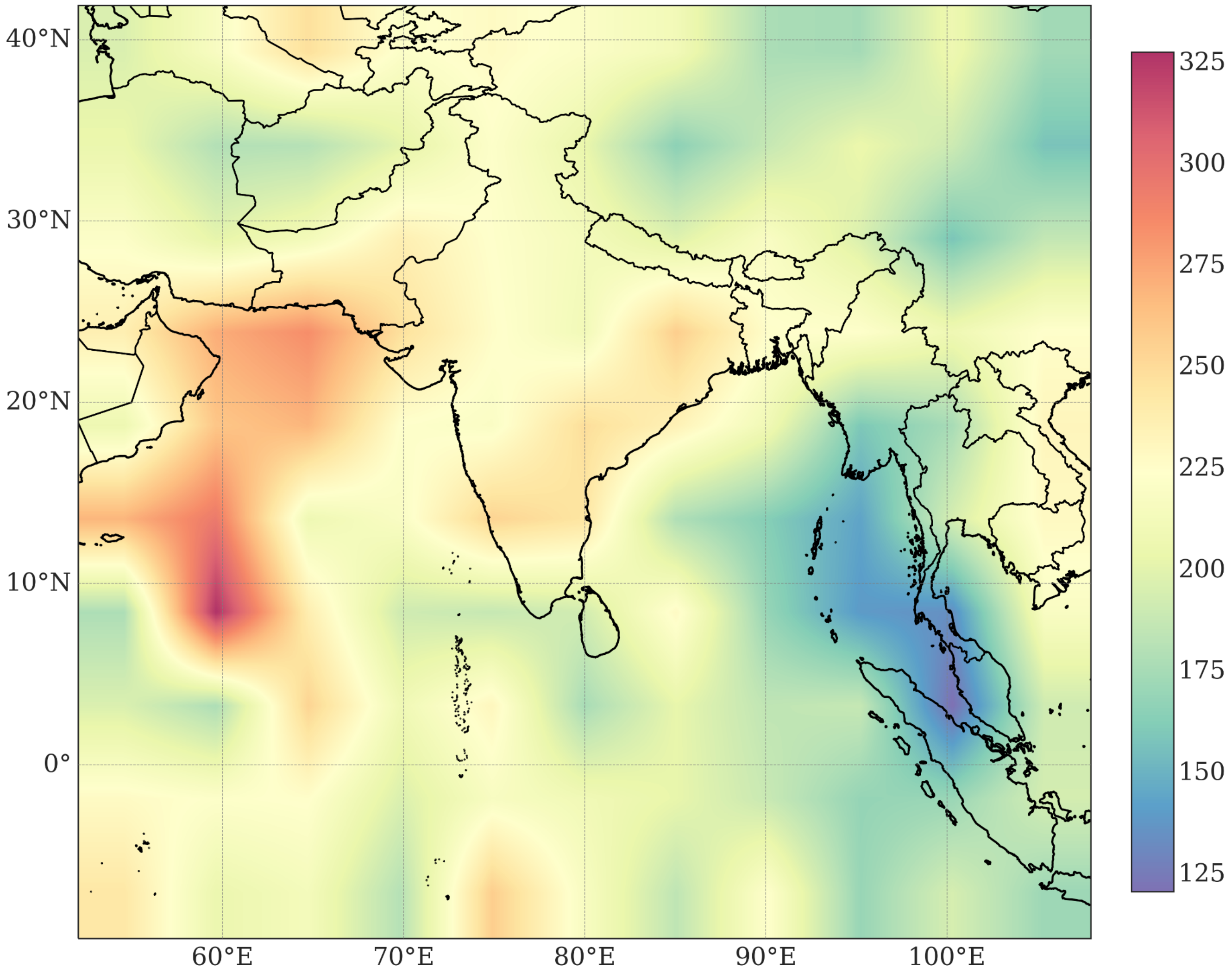

Figure 5. Spatial distribution of assimilated GNSS-RO profiles accumulated over the study period on a $5^{\circ} imes 5^{\circ}$ grid.

Relatively higher counts are observed over the Arabian Sea and along the east coast of India, where values reach about 300–350 profiles per 5° × 5° grid box. Over most other regions, the number of profiles ranges between about 150 and 250 per 5° × 5° grid box.

Figure 6 shows the histograms of observation-minus-background (O–B) and observation-minus-analysis (O–A) distributions from RMX-BA experiment. 180

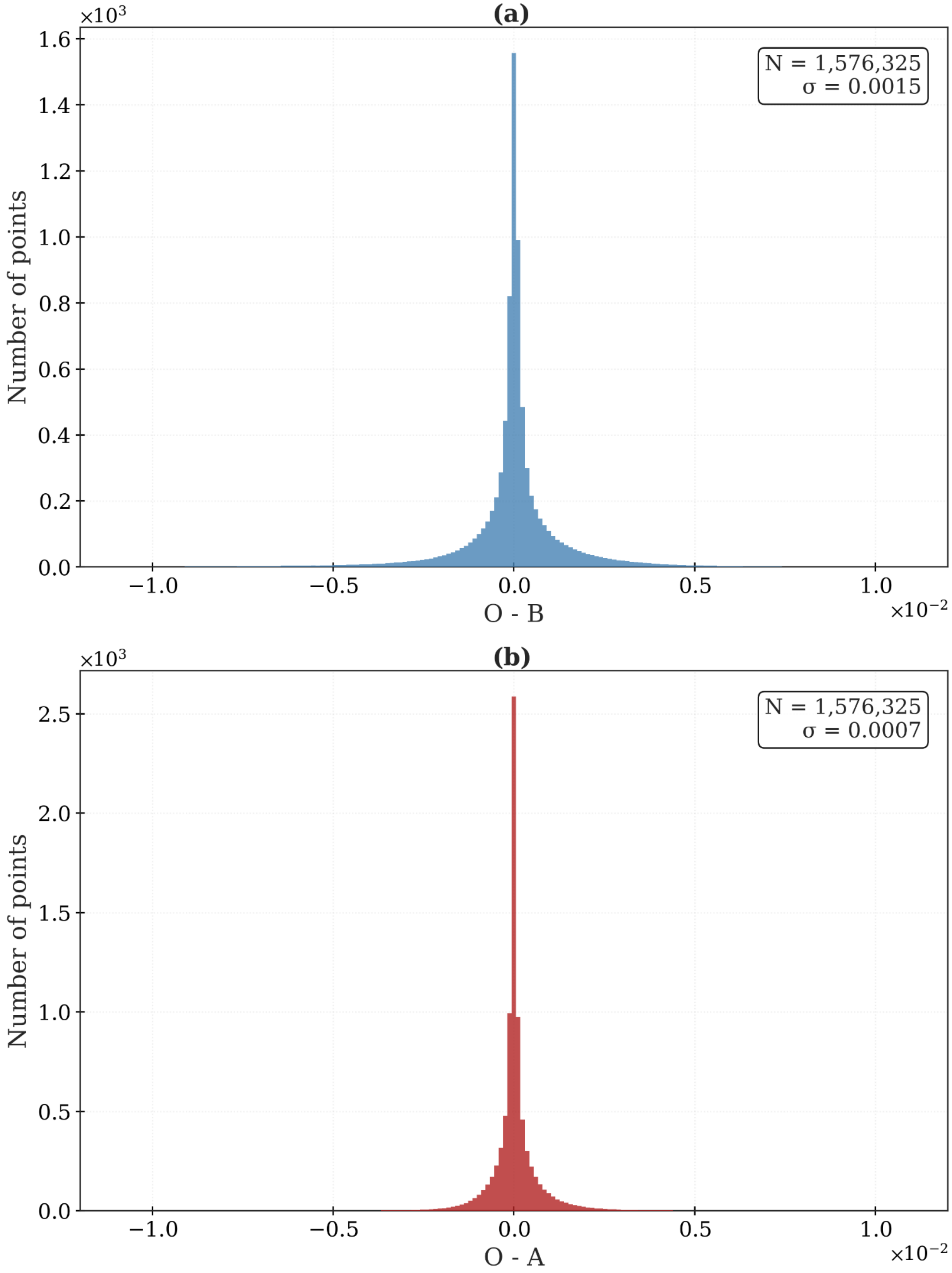

Figure 6. Histograms of observation-minus-background (O–B) and observation-minus-analysis (O–A) departures for assimilated bending-angle observations in the RMX-BA experiment.

https://doi.org/10.5194/egusphere-2026-2304
Preprint. Discussion started: 20 May 2026

The total number of assimilated bending angle observations is about 1.58 million. The standard deviation of the O–A departures (0.00070°) is about half the magnitude of the O–B departures (0.0015°), indicating a clear reduction in departures after assimilation. It should be noted that the quality control applied was very stringent, following the NCEP GSI operational assimilation system; hence, the observations were used conservatively.

3.2 Assessment of RO assimilation performance

During September 2022, a total of 120 analyses were produced in each experiment at 6-hour intervals. The model was integrated to generate 72-h forecasts daily from the 00 and 12 UTC analyses. Thus, a total of 60 forecasts of 72-h period were used to compute the error statistics.

To assess the impact of RO bending angle assimilation, the quality of the WRF analyses and subsequent forecasts of water vapor, temperature, and wind from both experiments was evaluated by comparison with ERA5 reanalysis, while precipitation forecasts were verified against Integrated Multi-satellite Retrievals for GPM (IMERG) rainfall estimates (Huffman et al., 2020). Standard verification metrics, including bias, root-mean-square difference (RMSD), and standard deviation differences (Std.Dev.), were computed for wind, temperature, and specific humidity at different pressure levels and forecast lead times. For rainfall, standard skill scores were calculated at various rainfall thresholds and forecast hours. In addition to these metrics, the moist total energy norm (TE) was used as an error measure. The TE is a vertically integrated index that combines contributions from pressure, temperature, wind, and water vapor, and is considered one of the most comprehensive single metrics for evaluating overall model performance (Ehrendorfer et al., 1999).

3.2.1 Evaluation using moist total energy norms

The domain-averaged moist total energy (TE) norm, computed by comparing the analyses and forecasts against the ERA5 reanalysis, is presented in Figure 7.

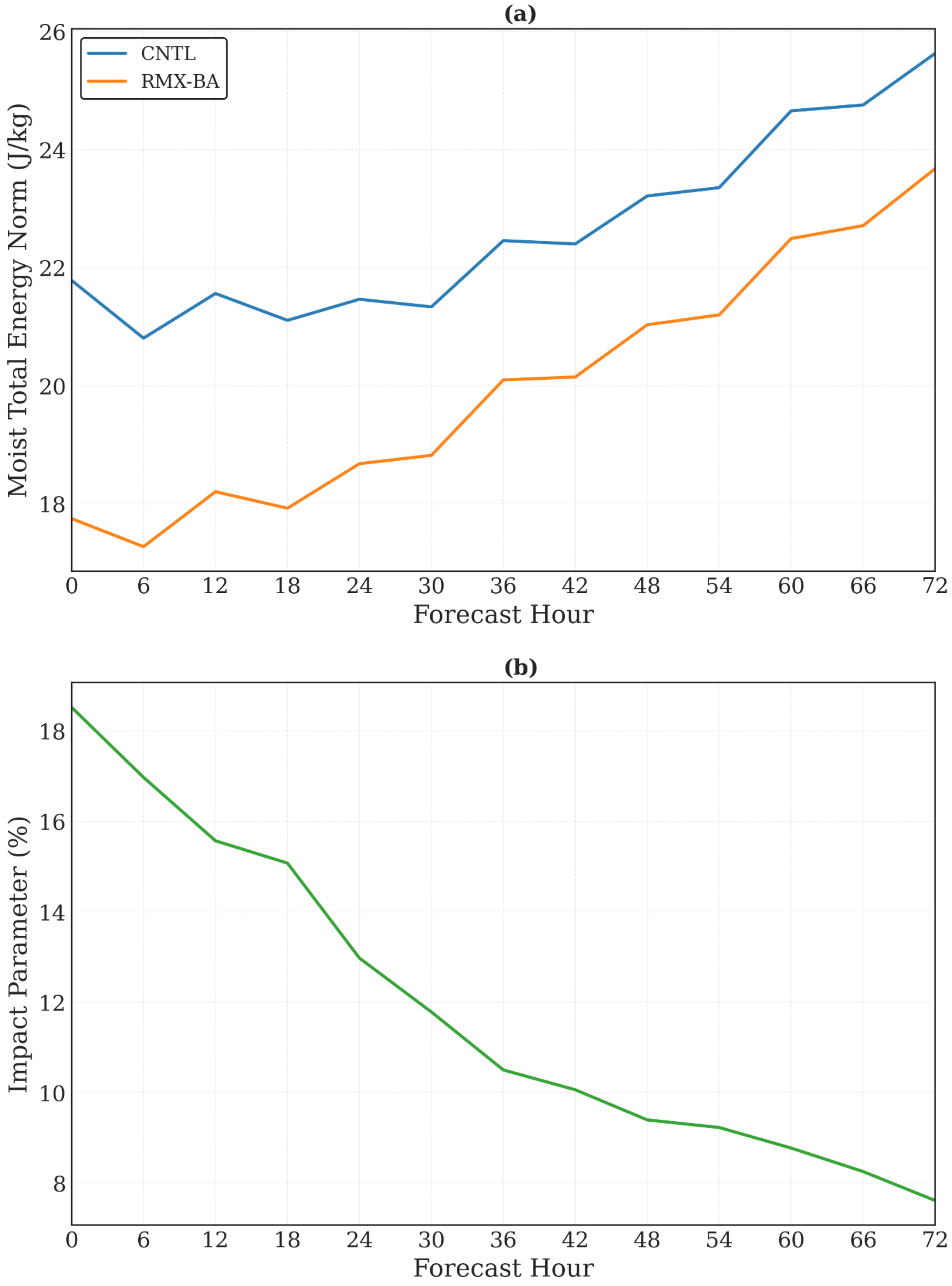

Figure 7. Domain-averaged moist total energy norm for CNTL and RMX-BA as a function of forecast lead time, together with the corresponding impact parameter derived from the total-energy norm.

Lower TE values correspond to smaller forecast errors. In the CNTL experiment, TE ranges between 21.8 and 27 J kg^{-1}, whereas in the RMX-BA experiment it varies from 17.5 to 24.5 J kg^{-1}. As expected, TE exhibits a systematic increase with forecast lead-time, with the minimum error observed at the analysis time (0-hour forecast) and the maximum error at the 72-h forecast (Fig.7a).

To assess the impact of RO assimilation, an Impact Parameter (IP) is defined (Eq. 5), representing the reduction in total energy (TE) error attributable to the inclusion of RO observations. Positive IP values denote a favourable impact of the RO data, while negative values indicate a deterioration of the forecast resulting from their assimilation.

$$IP = \frac{TE_{\text{CNTL}} - TE_{\text{RMX-BA}}}{TE_{\text{CNTL}}} \times 100 \tag{5}$$

TECNTL and TERMX-BA denote the total moist energy (TE) values in the CNTL and RMX-BA, respectively. The assimilation of RO observations leads to a consistent reduction in forecast errors across all lead times, with maximum improvements of 20% at analysis time, 15% at 24 hours, 10.5% at 48 hours, and 8.5% at 72 hours (Fig, 7b).

Figure 8 presents the spatial distribution of the TE Impact Parameter (IP) at various forecast lead times.

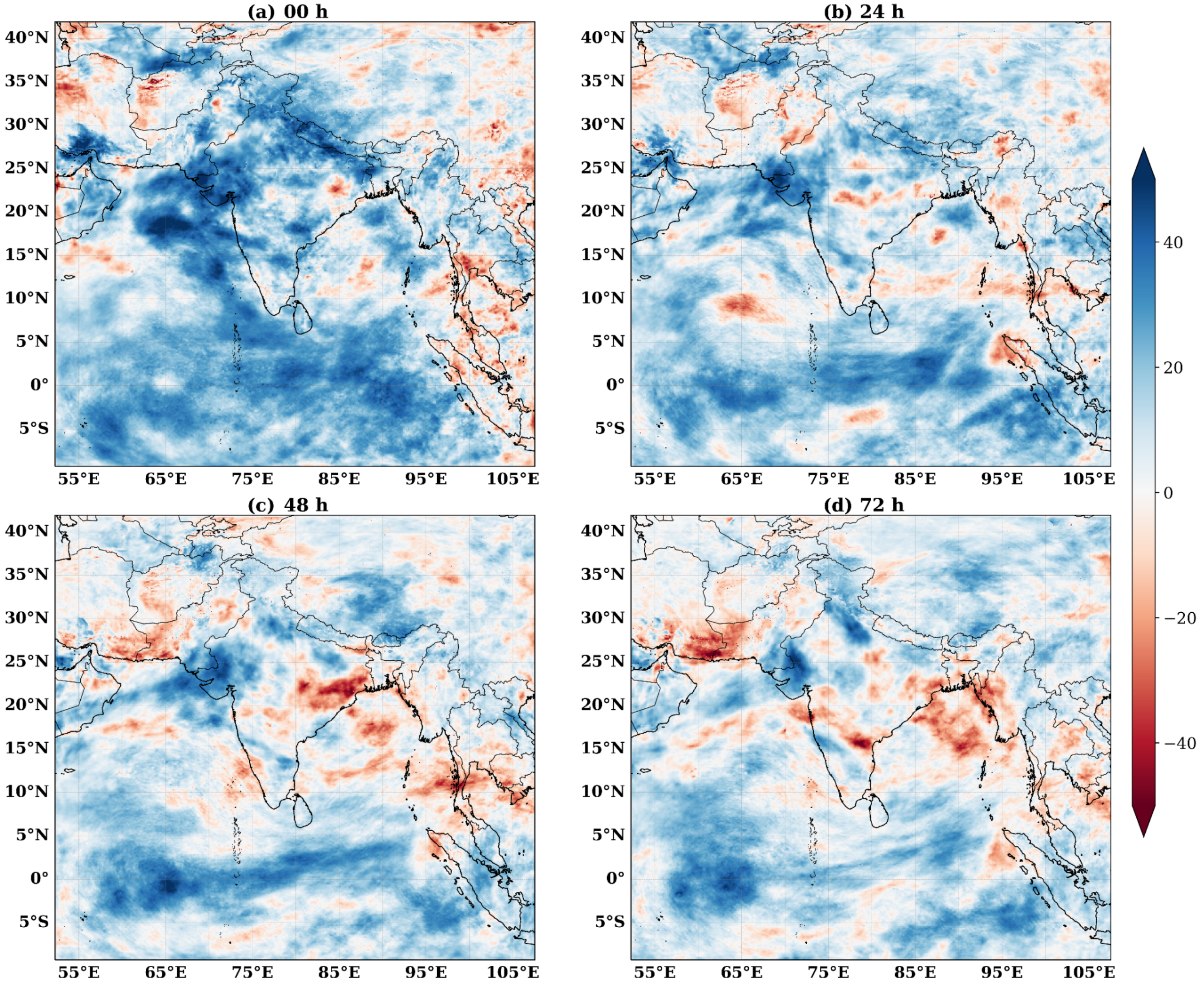

Figure 8. Spatial distribution of the total-energy impact parameter at forecast lead times of 00, 24, 48, and 72 h. Positive values indicate improvement due to RO assimilation.

The results indicate that a substantial portion of the domain exhibits positive IP values, with magnitudes reaching up to 40–50%, thereby demonstrating the beneficial impact of RO assimilation. The most pronounced reductions in TE are observed over the equatorial Indian Ocean, the northern Arabian Sea, parts of northwest India, and the Himalayan foothills. Some scattered pockets of degradation, ranging between 20-30%, are evident over the Bay of Bengal and at isolated location in eastern and western parts of the domain, predominately during later forecast hours.

3.2.2 Evaluation based on bias and error standard deviation

The impact of RO data assimilation on forecast accuracy was quantified using an impact parameter (IP) defined as the percentage reduction in standard deviation of errors between the CNTL and RMX-DA experiments, with ERA5 taken as the reference for verification.

$$IP = \frac{\sigma_{\text{CNTL}} - \sigma_{\text{RMX-BA}}}{\sigma_{\text{CNTL}}} \times 100 \qquad (6)$$

Where Std.Dev CNTL and Std.Dev RMX-DA represent standard deviations of the forecast error for the CNTL and RMX-DA experiments, respectively, computed with respect to the ERA5 analysis. Positive values of IP indicate an improvement (reduction in error) due to RO assimilation, while negative values indicate degradation.

Figure 9 shows the domain-averaged forecast error from the control experiment (Std.Dev CNTL) at 00, 24, 48 and 72 hours, evaluated across different vertical levels for specific humidity, temperature and wind.

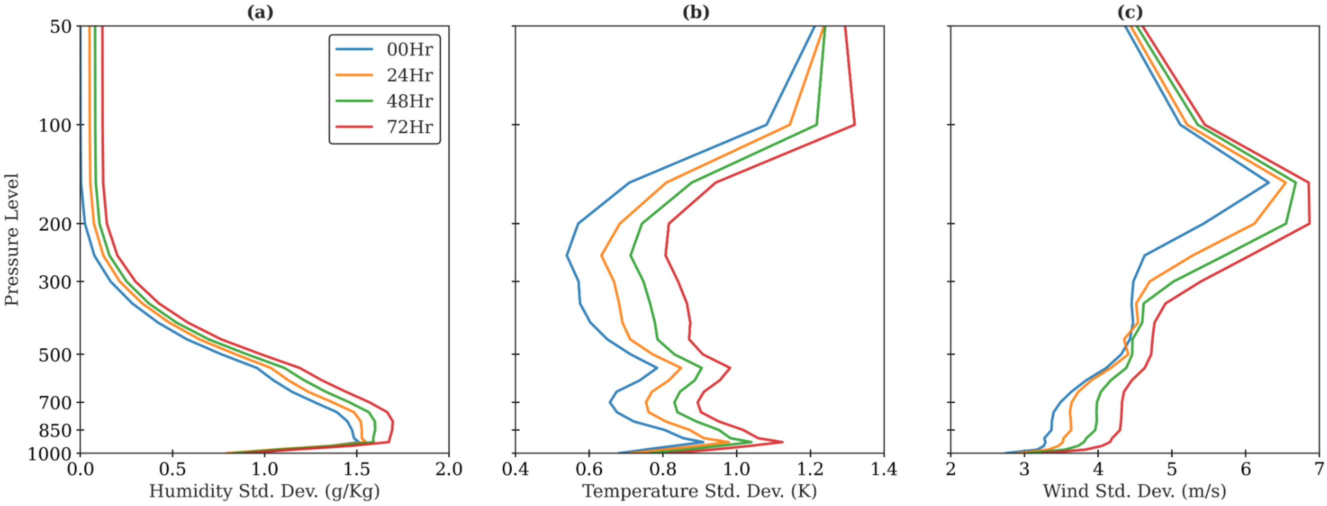

Figure 9. Domain-averaged forecast-error standard deviation in CNTL for specific humidity, temperature, and wind at 00, 24, 48, and 72 h.

The specific humidity error is maximum (1–1.5 g kg^{-1}) near the surface and around 850 hPa. Temperature errors range from 0.6 K to 1.2 K, with maximum errors observed at 100 hPa and near the surface. Wind errors vary between 3 and 6.8 m s^{-1}, with the largest errors occurring at 100 hPa. The errors of all variables increase with forecast length. Figure 10 presents the domain-averaged IP for specific humidity (Fig 10a), temperature (Fig.10b), and wind (Fig 10c) at different pressure levels and forecast lead times.

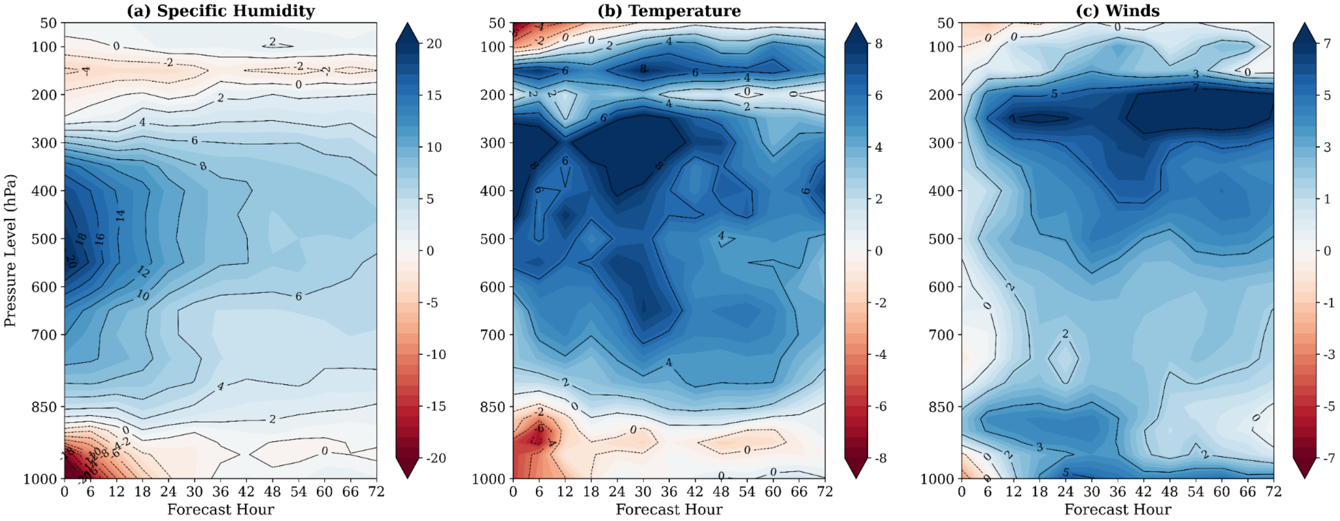

Figure 10. Domain-averaged impact parameter based on error standard deviation for specific humidity, temperature, and wind as a function of pressure level and forecast lead time.

A positive impact of up to 15–20% in specific humidity and about 8–12% in temperature and winds is evident with the assimilation of RO data. For specific humidity, the impact is largest during the initial forecast hours and decreases to about 10% by the end of the 72-h forecast. The greatest impact is observed in the 850–300 hPa layer. For temperature, the impact is strongest in the middle troposphere and remains fairly consistent, generally in the range of 6–12%. In the case of winds, the maximum impact is found near 250 hPa, and the impact tends to increase with forecast lead time. The forecast improvements are larger in magnitude than those in the analysis. It should be noted that the assimilation of RO observations can improve winds in data assimilation and NWP through several physical and dynamical mechanisms. Two primary mechanisms contribute to this improvement. First, through geostrophic adjustment, changes in pressure and temperature fields resulting from RO observations can lead to adjustments in the wind fields. Second, water vapor changes induced by RO observations can influence precipitation and convection through latent heat release. Improved representation of water vapor leads to better simulation of precipitation processes, and the associated latent heat release modifies atmospheric stability and vertical motion. These changes can alter pressure gradients, which in turn influence wind fields

Overall, the impact remains positive for most variables across the majority of pressure levels, with only minor degradation observed near the surface and during the initial forecast lead times, mainly in specific humidity and temperature. A small negative impact is also noted in the upper tropospheric specific humidity around 150 hPa.

Figure 11 illustrates the vertical variation of the domain-averaged bias between ERA5 and the WRF model forecasts of specific humidity at the analysis time and at the 72-h forecast (Fig. 11a).

https://doi.org/10.5194/egusphere-2026-2304
Preprint. Discussion started: 20 May 2026

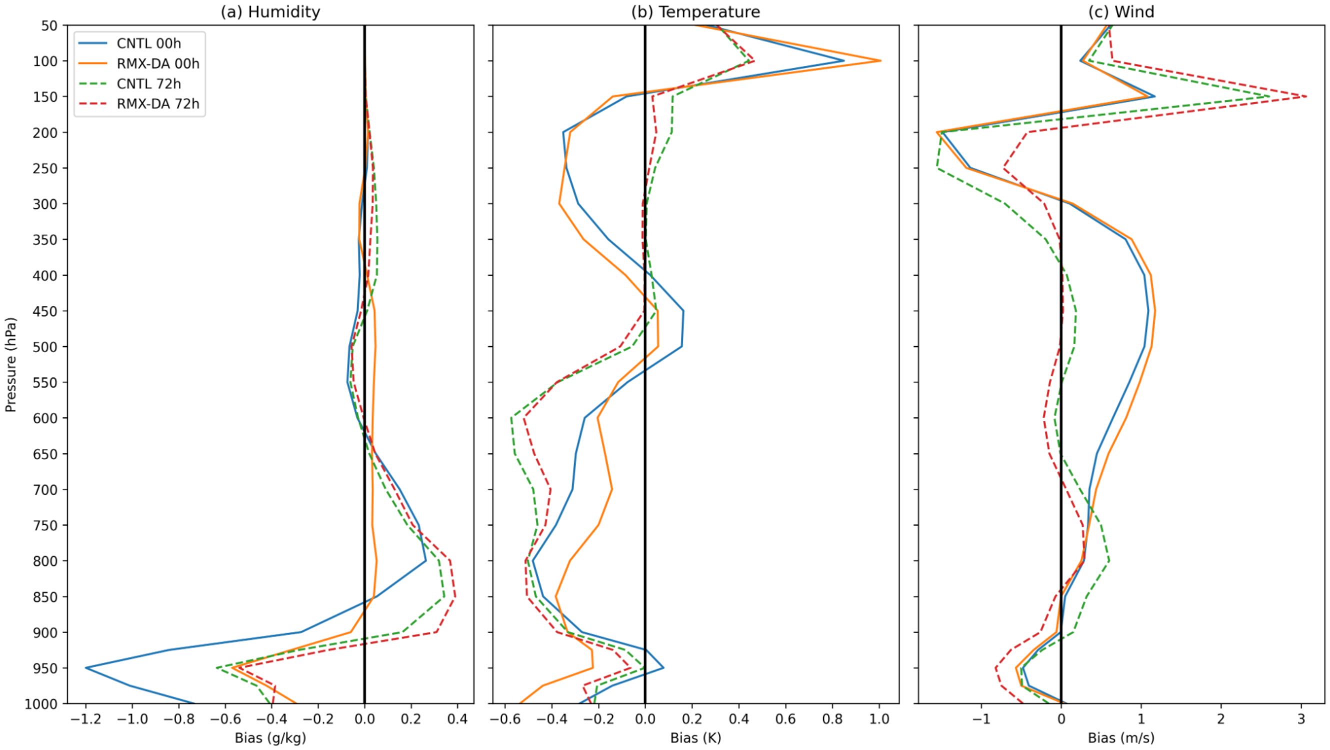

Figure 11. Vertical profiles of domain-averaged bias relative to ERA5 for CNTL and RMX-BA at analysis time and 72 h forecast time for specific humidity, temperature, and wind.

At the analysis time, in the CNTL experiment, the model exhibits a pronounced overestimation of specific humidity in the lower troposphere, reaching up to 1.4 g kg^{-1}, while an underestimation of approximately 0.5 g kg^{-1} is observed in the layer between 850 and 700 hPa. The assimilation of RO data in the RMX-BA experiment leads to a substantial reduction in these biases. Following assimilation, the mean bias is reduced to within ± 0.5 g kg^{-1} across most of the troposphere. The positive impact on bias is evident up to the 24-hour forecast lead time; beyond this range, the biases in both the CNTL and RO assimilation experiments become broadly comparable. At longer forecast lead times, the RMX-BA experiment exhibits slightly higher biases near 850 hPa and marginally lower biases in the lower and middle troposphere relative to the CNTL experiment

The temperature biases range between -0.5 and 1.1K and appear broadly similar in both the CNTL and RMX-BA experiments (Fig. 11b). At some pressure levels, the RMX-BA experiment demonstrates improved performance, whereas at others, the control run exhibits marginally lower biases. This pattern remains similar across all forecast lead times; however, the overall magnitude of the biases decreases with increasing lead time, reducing to ± 0.66 K at the 72-hour forecast.

The wind biases vary between -1.5 and 1.5 m s^{-1} and are largely comparable in both the control and RO assimilation experiments (Fig. 11c). As the forecast lead time increases, the magnitude of the biases also increases, reaching values between -3 and 3 m s^{-1}. Furthermore, the biases in the RO assimilation experiment are slightly higher than those in the control run at most levels, except at 800 hPa and 150 hPa, during the later forecast hours.

265 Figure 11a clearly demonstrates a substantial reduction in the specific humidity bias of the analysis following the assimilation of RO bending angle observations. To identify the regions where this reduction is most pronounced, the spatial distribution of humidity biases at 850 and 500 hPa for both the CNTL and RMX-BA experiments is presented in Figure 12. Figure 12 indicates that the CNTL experiment strongly underestimates lower-tropospheric specific humidity over large parts of the Arabian Sea, the Bay of Bengal, and the southern Indian Ocean, while overestimating specific humidity over several land regions.

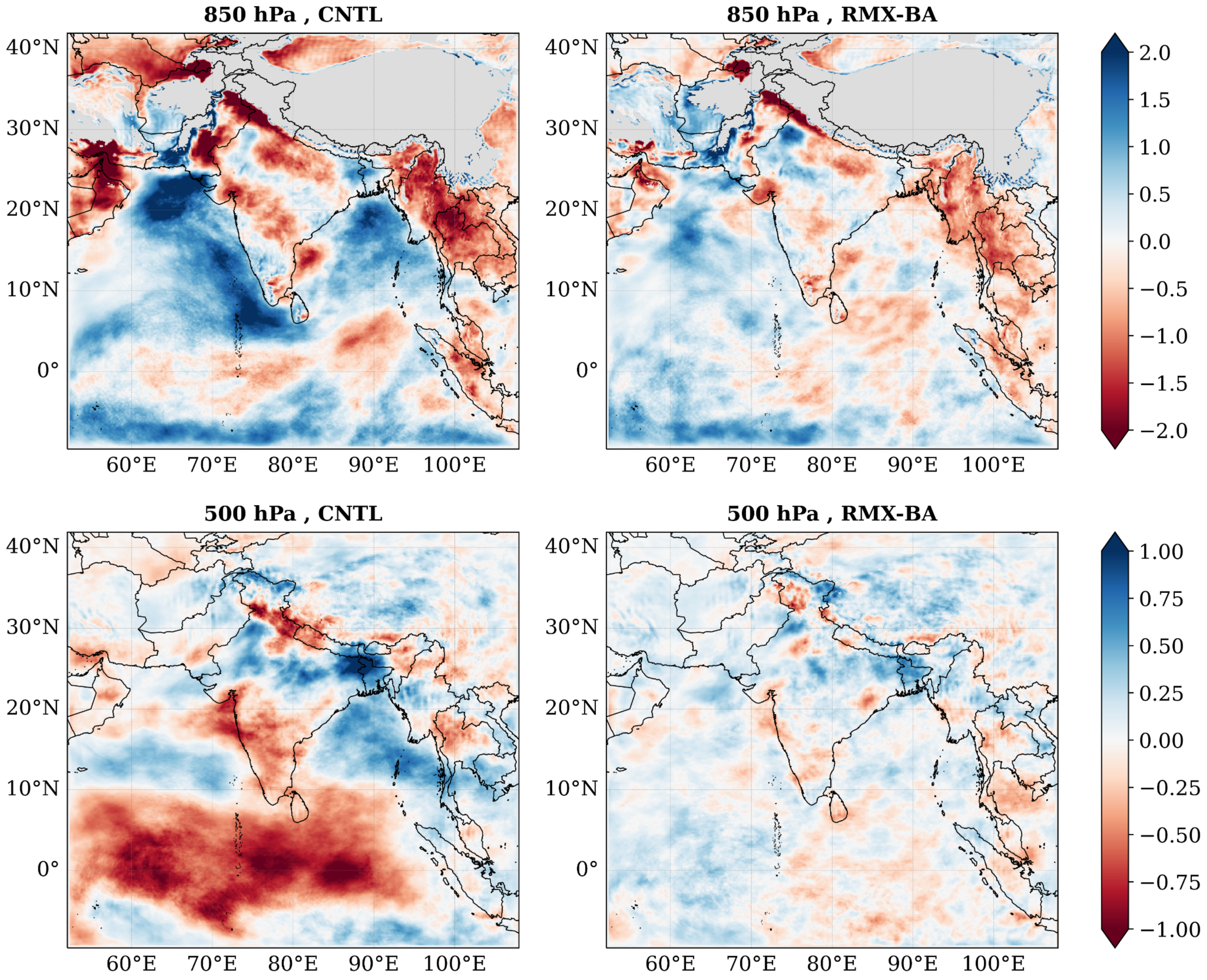

Figure 12. Spatial distribution of specific-humidity bias relative to ERA5 at 850 and 500 hPa for CNTL and RMX-BA.

270 The underestimation and overestimation in CNTL ranges from ± 2 g kg-1 at 850 h Pa and from ± 1 g kg-1 at 500 hPa. The assimilation of RO data substantially reduces these biases in the 850 hPa specific humidity field. At 500 hPa, the CNTL experiment exhibits a marked overestimation of specific humidity over the equatorial Indian Ocean and an underestimation

over the Bay of Bengal, eastern India, and northwestern India. The assimilation of RO data significantly mitigates these biases. In the RO assimilation experiment, the magnitude of the bias remains within ± 1 g kg-1 at 850 hPa and ± 0.5 g kg-1 at 500 275 hPa.

3.2.3 Evaluation of rainfall prediction skill

Figure 13 shows the spatial distribution of the monthly-accumulated rainfall for September 2022 based on 24-h forecasts from the CNTL experiment (Fig.13a).

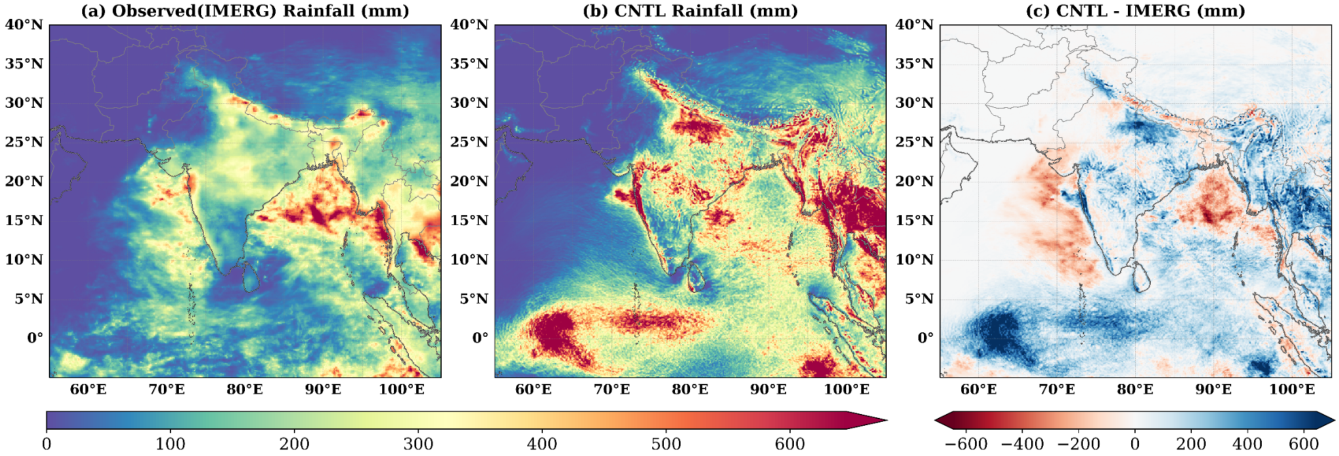

Figure 13. September 2022 monthly accumulated rainfall from IMERG, from CNTL 24 h forecasts, and the corresponding CNTL minus IMERG difference.

Model-predicted rainfall is verified against rainfall estimates from the Integrated Multi-Retrievals for GPM (IMERG) product (Huffman et al., 2020) (Fig.13b). Figure 13 indicates that the model underestimates rainfall, by as much as 200-500 mm, over the Bay of Bengal, the eastern Arabian Sea, and along the west coast of India (Fig.13c). In contrast, rainfall is strongly overestimated, by as much as 200-600 mm, over the equatorial Indian Ocean, particularly the western equatorial Indian Ocean, as well as over some parts of India and the eastern portion of the domain (Fig. 13c). These large discrepancies in rainfall prediction correspond well with the regions of substantial humidity biases at 850 and 500 hPa, as noted in Figure 12.

$$IP = \frac{\left|Rain^{\text{CNTL}} - Rain^{\text{IMERG}}\right| - \left|Rain^{\text{RMX-BA}} - Rain^{\text{IMERG}}\right|}{\left|Rain^{\text{CNTL}} - Rain^{\text{IMERG}}\right|} \times 100 \tag{7}$$

$Rain^{\text{IMERG}}$ and $Rain^{\text{RMX-BA}}$ represent the model-predicted rainfall in the control and RO assimilation experiments, respectively, while $Rain^{\text{IMERG}}$ provides the observed rainfall. Figure 14 presents the spatial distribution of the impact parameter (IP).

https://doi.org/10.5194/egusphere-2026-2304
Preprint. Discussion started: 20 May 2026

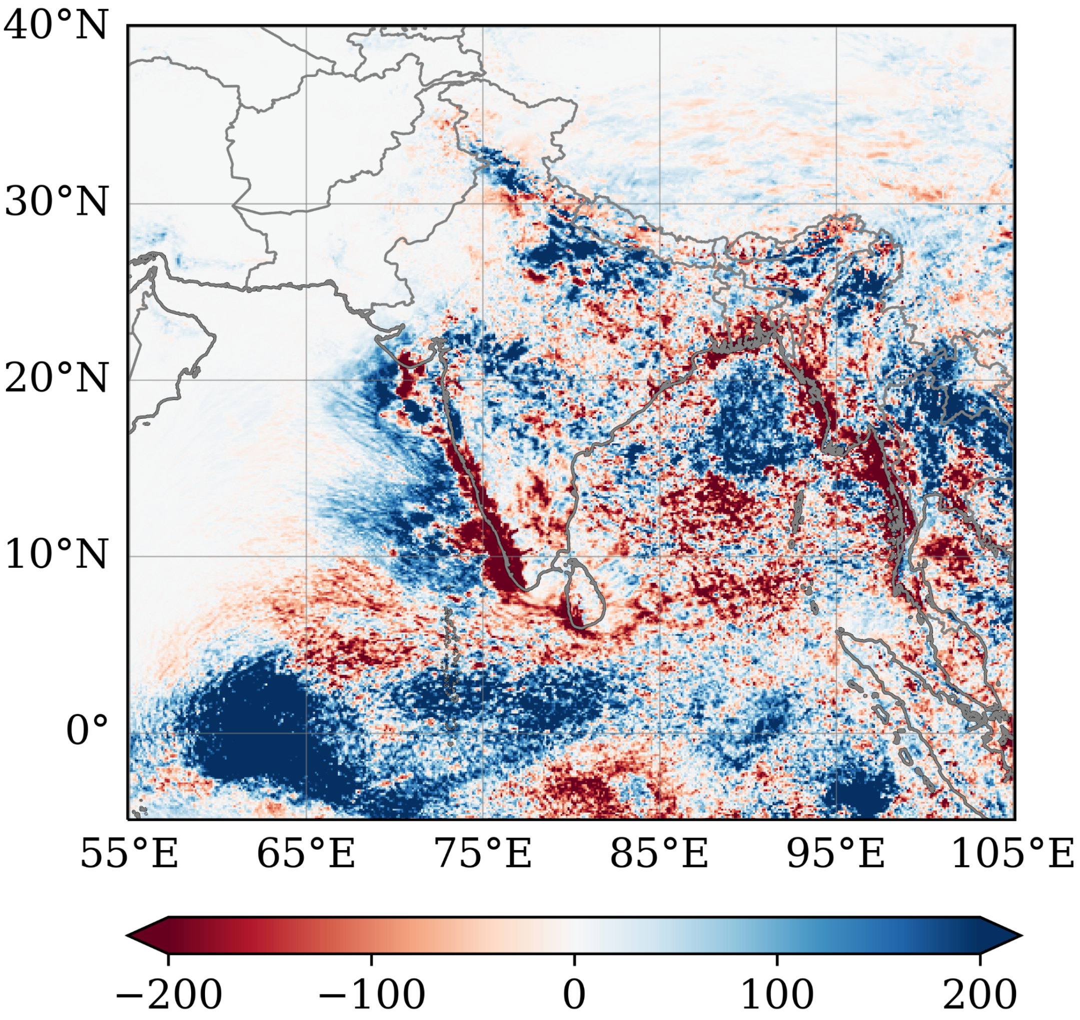

Figure 14. Spatial distribution of the rainfall impact parameter. Positive values denote reduced rainfall error due to RO assimilation.

Positive values of IP indicate improved rainfall prediction due to RO assimilation, whereas negative values indicate degradation. Most of the domain is characterized by positive IP values, indicating an overall improvement in rainfall prediction with RO assimilation. Significant improvements are observed over the equatorial Indian Ocean, the Arabian Sea, the Bay of Bengal, and much of the Indian landmass. The underestimation/overestimation of rainfall is reduced by as much as 200-300 mm with the assimilation of RO observation. This improvement is likely associated with enhanced water vapor analysis resulting from the assimilation of RO observations.

However, some localised regions exhibit degradation in rainfall prediction following RO assimilation, primarily over the Western Ghats and along the eastern Bay of Bengal, with a few isolated pockets over adjacent oceanic areas. IMERG rainfall estimates are generally less reliable over complex terrain, particularly mountainous regions such as the Western Ghats, as well as over coastal and convectively active regions such as the eastern Bay of Bengal (Prakash et al., 2021; Tan et al., 2017),

https://doi.org/10.5194/egusphere-2026-2304
Preprint. Discussion started: 20 May 2026

which may partly account for the apparent degradation associated with RO assimilation. Overall, RO assimilation leads to a
300 substantial improvement in rainfall prediction, especially in regions where the CNTL exhibited the largest errors.

Furthermore, rainfall skill scores—specifically the equitable threat score (ETS) and bias score—were computed to gain deeper insight into the impact of RO data on rainfall prediction skill. The ETS and bias are calculated for 24- and 48-h model predicted rainfall using IMERG rainfall as the reference dataset. Figure 15 presents the ETS and bias scores for 24-hour and 48-hour accumulated rainfall at various rainfall thresholds.

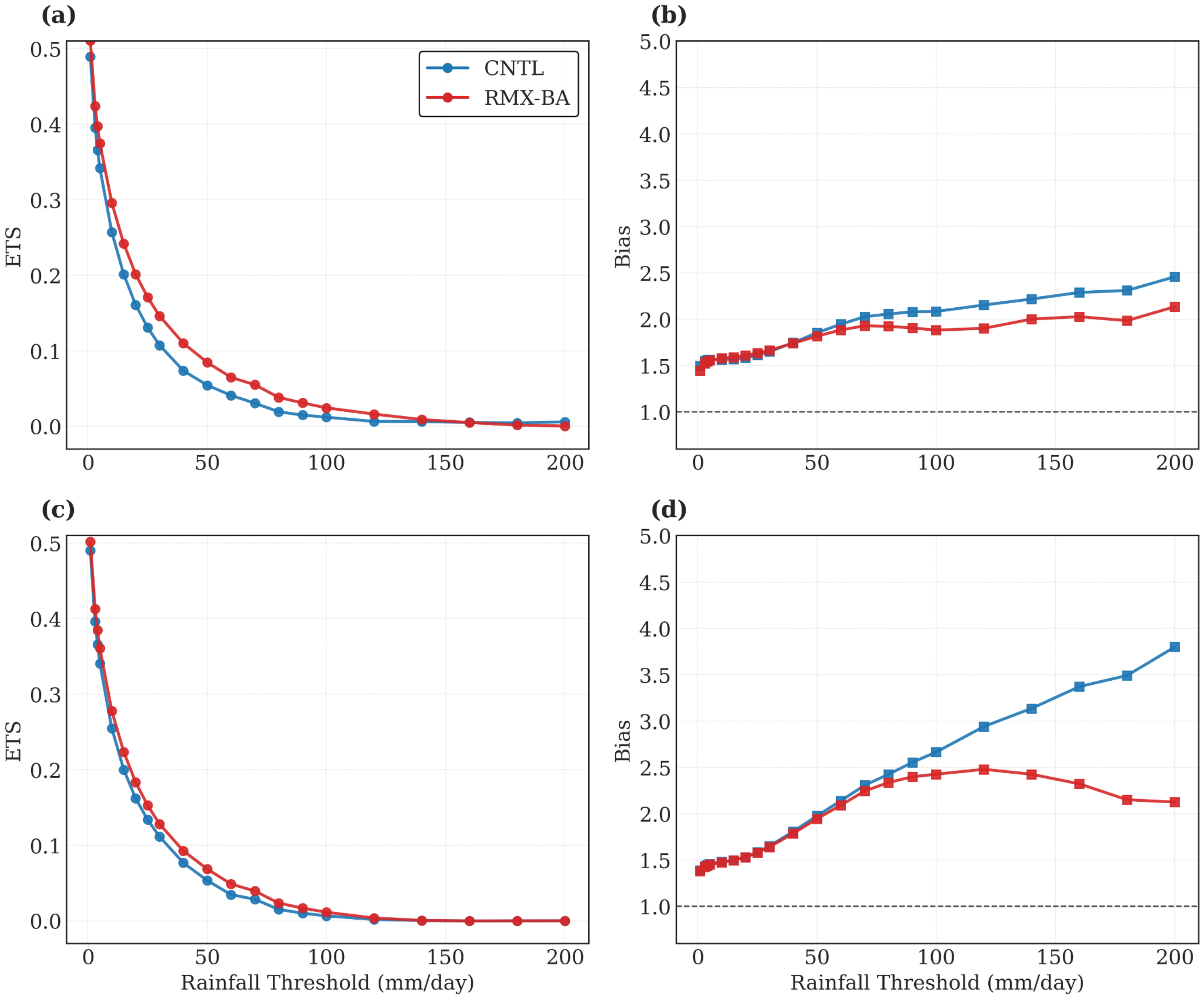

Figure 15. Equitable threat score (ETS) and bias score for 24 and 48 h accumulated rainfall as a function of rainfall threshold for CNTL and RMX-BA.

Both ETS and bias scores should be close to 1 for a perfect forecast. A bias score greater than 1 indicates that the model overestimates rainfall occurrence, while a bias score less than 1 indicates an underestimation of rainfall occurrence. The results clearly show that both ETS and bias scores improve with the assimilation of RO data. The ETS exhibits a substantial improvement for 24-h accumulated rainfall forecasts. The bias scores also show significant improvement, with the largest improvement observed in the 48-h forecasts.

4 Conclusions

This study evaluated the impact of assimilating RO bending angle observations from the ROMEX dataset on mesoscale weather prediction over the Indian region during September 2022. The data assimilation and forecast experiments were conducted using the WRF model and its three-dimensional variational (3D-Var) data assimilation system. A bending angle observation operator was integrated into the WRF data assimilation system, enabling the direct assimilation of bending angle observations and improved use of RO measurement information.

Cycling 3D-Var experiments were conducted at 9-km horizontal resolution using the WRF model to assess the impact of ROMEX RO bending angle assimilation. The results indicate that the assimilation of RO data leads to consistent improvements in both the analysis fields and subsequent forecasts. These improvements are evident in the representation of thermodynamical and dynamical variables, highlighting the added value of RO observations in improving model performance.

RO assimilation leads to a clear reduction in both analysis and forecast errors, as reflected in the verification metrics. Moist Total Energy (TE) error reductions of about 20 % at analysis time indicate that bending angle observations effectively constrain the model's initial state. Although the impact decreases with forecast lead time, improvements of about 8–9 % remain up to 72 hours.

The largest benefit of RO assimilation is observed in the water vapor field. Specific humidity in the middle troposphere shown an improvement of 15-20%. Specific humidity biases are reduced across much of the troposphere, particularly over oceanic regions where conventional observations are sparse. The assimilation corrects both moist and dry biases, resulting in a more realistic representation of the water vapor distribution. Temperature and wind fields also show improvement (10 to 12%), although to a lesser extent, with the most noticeable impact on winds occurring in the upper troposphere.

Rainfall forecasts show substantial improvement with the assimilation of RO data. Regions exhibiting reduced rainfall error closely corresponds to areas where humidity biases are reduced, underscoring the importance of accurate water vapor initialisation. Skill-score verification indicates improvements in both ETS and bias.

The results highlight the significant value of high-density RO observations for mesoscale forecasting over the Indian monsoon region, where conventional observations are sparse. Overall, the findings demonstrate that the assimilation of a large number of RO bending angle observations can significantly improve regional weather prediction.

Code availability. The WRF model and WRF-DA system used in this study are publicly available from the NCAR repository. The Radio Occultation Processing Package (ROPP) is available from ROM SAF. The code modifications used to couple the bending-angle operator with WRF-DA are not publicly archived but can be provided by the corresponding author upon request.

Data availability. The datasets used in this study are publicly available. GNSS radio occultation (GNSS-RO) observations from the ROMEX mission were obtained from the EUMETSAT ROM SAF (https://www.romsaf.org). Meteorological reanalysis data were taken from the ERA5 dataset provided by the Copernicus Climate Data Store (CDS) (https://cds.climate.copernicus.eu). Conventional PREPBUFR observational data were obtained from the Data Support Section (DSS) of the National Center for Atmospheric Research (NCAR), managed by UCAR (https://rda.ucar.edu). IMERG rainfall data were obtained from NASA's Global Precipitation Measurement (GPM) mission (https://gpm.nasa.gov/data/imerg).

Author contributions. Randhir Singh led the study, carried out the data assimilation experiments, and prepared the initial manuscript draft. Satya P. Ojha and Kudilil Faisal Muhammed contributed to the methodology, analysis, and manuscript revision. Richard Anthes contributed to the scientific interpretation of the ROMEX experiment and manuscript revision. All authors discussed the results and approved the manuscript.

Competing interests. The contact author has declared that none of the authors has any competing interests.

Acknowledgements. The authors sincerely acknowledge the encouragement and support provided by the Group Director, AOSG/EPSA/SAC; the Deputy Director, EPSA/SAC; and the Director, Space Applications Centre (SAC). The use of the WRF model is gratefully acknowledged. The ROPP software was obtained from the EUMETSAT Radio Occultation Meteorology Satellite Application Facility (ROM SAF).

References

Anthes, R. A., Marquardt, C., Ruston, B., and Shao, H.: Radio Occultation Modelling Experiment (ROMEX)—Determining the impact of radio occultation observations on numerical weather prediction, Bull. Am. Meteorol. Soc., 105, https://doi.org/10.1175/BAMS-D-23-0326.1, 2024.

Anthes, R. A., Rocken, C., and Kuo, Y.-H.: Applications of COSMIC to meteorology and climate, Terr. Atmos. Ocean. Sci., 11, 115–156, https://doi.org/10.3319/TAO.2000.11.1.115(COSMIC), 2000.

Anthes, R. A., Bernhardt, P. A., Chen, Y., Cucurull, L., Dymond, K. F., Ector, D., Healy, S. B., Ho, S.-P., Hunt, D. C., Kuo, Y.-H., et al.: The COSMIC/FORMOSAT-3 mission: Early results, Bull. Am. Meteorol. Soc., 89, 313–334, https://doi.org/10.1175/BAMS-89-3-313, 2008.

Anthes, R. A., Sjoberg, J., Starr, J., and Zeng, Z.: Evaluation of biases and uncertainties in ROMEX radio occultation observations, Atmos. Meas. Tech., 18, 6997–7019, https://doi.org/10.5194/amt-18-6997-2025, 2025.

Aparicio, J. M., and Deblonde, G.: Signature of the atmospheric compressibility factor in COSMIC, CHAMP, and GRACE radio occultation data, J. Geophys. Res. Atmos., 114, D16114, https://doi.org/10.1029/2008JD011156, 2009.

Barker, D. M., et al.: The Weather Research and Forecasting Model's Community Variational/Ensemble Data Assimilation System: WRFDA, Bull. Am. Meteorol. Soc., 93, 831–843, https://doi.org/10.1175/BAMS-D-11-00167.1, 2012.

Bowler, N.E.: An assessment of GNSS radio occultation data produced by Spire. Q. J. R. Meteor. Soc., 146, 3772-3788, https://doi.org/10.1002/qj.3872 , 2020.

Cardinali, C. and S. Healy, Impact of GPS radio occultation measurements in the ECMWF system. Q. J. R. Meteor. Soc., 140, 2315-2320, https://doi.org/10.1002/qj.2300, 2014.

Chen, S. Y., Huang, C. Y., Kuo, Y. H., Guo, Y. R., and Sokolovskiy, S.: Assimilation of GPS refractivity from FORMOSAT-3/COSMIC using a nonlocal operator with WRF 3DVAR and its impact on typhoon prediction, Terr. Atmos. Ocean. Sci., 20, 133–154, https://doi.org/10.3319/TAO.2007.11.29.01(F3C), 2009.

Cucurull, L., Derber, J. C., and Purser, R. J.: A bending angle forward operator for GPS radio occultation measurements, J. Geophys. Res. Atmos., 118, 14–28, https://doi.org/10.1029/2012JD017782, 2013.

Cucurull, L., Derber, J. C., Treadon, R., and Purser, R. J.: Assimilation of Global Positioning System radio occultation observations into NCEP's Global Data Assimilation System, Mon. Weather Rev., 135, 3174–3193, https://doi.org/10.1175/MWR3461.1, 2007.

Culverwell, I. D., et al.: The Radio Occultation Processing Package (ROPP), Atmos. Meas. Tech., 8, 1887–1901, https://doi.org/10.5194/amt-8-1887-2015, 2015.

Ehrendorfer, M., Errico, R. M., and Raeder, K. D.: Singular vector perturbation growth in a primitive equation model with moist physics, J. Atmos. Sci., 56, 1627–1648, https://doi.org/10.1175/1520-0469(1999)056<1627:SVPGIA>2.0.CO;2 , 1999.

Eyre, J. R.: Assimilation of radio occultation measurements into a numerical weather prediction system, ECMWF Tech. Memo., 199, ECMWF, Reading, UK, https://www.ecmwf.int/en/elibrary/74433-assimilation-radio-occultation-measurements-numerical-weather-predictionsystem, 1994.

Geer, A. J., Lonitz, K., Weston, P., Kazumori, M., Okamoto, K., Zhu, Y., Liu, E. H., Collard, A., Bell, W., Migliorini, S., Chambon, P., Fourrie, N., Kopken-Watts, C., and Schraff, C.: All-sky satellite data assimilation at operational weather forecasting centres, Q. J. R. Meteorol. Soc., 144, 1191–1217, https://doi.org/10.1002/qj.3202, 2018.

Hersbach, H., et al.: The ERA5 global reanalysis, Q. J. R. Meteorol. Soc., 146, 1999–2049, https://doi.org/10.1002/qj.3803, 2020.

Healy, S. B.: Radio occultation bending angle and impact parameter errors caused by horizontal refractive index gradients in the troposphere: A simulation study, J. Geophys. Res. Atmos., 106, 11875–11889, https://doi.org/10.1029/2001JD900050, 2001.

Healy, S. B., and Thepaut, J.-N.: Assimilation experiments with CHAMP GPS radio occultation measurements, Q. J. R. Meteorol. Soc., 132, 605–623, https://doi.org/10.1256/qj.04.182, 2006.

Healy, S. B., Eyre, J. R., Hamrud, M., and Thepaut, J.-N.: Assimilating GPS radio occultation measurements with two-dimensional bending angle observation operators, Q. J. R. Meteorol. Soc., 133, 1213–1227, https://doi.org/10.1002/qj.63, 2007.

Hong, T.-X., Huang, C.-Y., Lin, C.-Y., Lien, G.-Y., Huang, Z.-M., and Chen, S.-Y.: Impacts of GNSS RO data on typhoon forecasts using global FV3GFS with GSI 4DEnVar, Atmosphere, 14, 735, https://doi.org/10.3390/atmos14040735, 2023.

Huang, C.-Y., Kuo, Y.-H., Chen, S.-Y., Terng, C. T., Chien, F. C., Lin, P. L., Kueh, M. T., Chen, S. H., Yang, M. J., and Wang, C. J.: Impact of GPS radio occultation data assimilation on regional weather predictions, GPS Solut., 14, 35–49, https://doi.org/10.1007/s10291-009-0144-1, 2010.

Huffman, G. J., et al.: Integrated multi-satellite retrievals for the Global Precipitation Measurement (GPM) mission (IMERG), in: Satellite Precipitation Measurement, Springer, https://doi.org/10.1007/978-3-030-24568-9_19, 2020.

Johnston, B. R., Cucurull, L., Anthes, R., Mueller, M. J., and Lim, A. H. N.: The impact of assimilating GNSS-RO observations on HAFS tropical cyclone forecasts from the 2022 Atlantic hurricane season, Weather Forecast., 40, 2539–2559, https://doi.org/10.1175/WAF-D-25-0045.1, 2025.

Kleist, D. T., Parrish, D. F., Derber, J. C., Treadon, R., Wu, W.-S., and Lord, S.: Introduction of the Gridpoint Statistical Interpolation (GSI) into the NCEP Global Data Assimilation System, Weather Forecast., 24, 1691–1705, https://doi.org/10.1175/2009WAF2222201.1, 2009.

Kursinski, E. R., et al.: Observing Earth's atmosphere with radio occultation measurements using the Global Positioning System, J. Geophys. Res., 102, 23429–23465, https://doi.org/10.1029/97JD01569, 1997.

Lin, H., Kuo, Y., Zhang, H., Braun, J., and Liu, Z.: Impact of GNSS RO data on the prediction of atmospheric river events: A ROMEX experiment, Weather Forecast., 41, 519–539, https://doi.org/10.1175/WAF-D-25-0151.1, 2026.

Liu, Y., and Xue, J.: Assimilation of GNSS radio occultation observations in GRAPES, Atmos. Meas. Tech., 7, 3935–3946, https://doi.org/10.5194/amt-7-3935-2014, 2014.

Lonitz, K., Vitart, F., Healy, S. B., and Fu, Q.: Sub-seasonal impact of GNSS radio occultation data, Geophys. Res. Lett., 52, e2025GL116068, https://doi.org/10.1029/2025GL116068, 2025.

Miller, W. J., Chen, Y., Ho, S.-P., and Shao, X.: Evaluating the impacts of COSMIC-2 GNSS RO bending angle assimilation on Atlantic hurricane forecasts using the HWRF model, Mon. Weather Rev., 151, 1821–1847, https://doi.org/10.1175/MWR-D-22-0198.1, 2023.

Miller, W. J., Chen, Y., Ho, S.-P., and Shao, X.: How does assimilating a large commercial GNSS RO dataset impact HAFS hurricane forecasts? An evaluation in support of the ROMEX experiment, EGUsphere [preprint], https://doi.org/10.5194/egusphere-2026-1000, 2026.

Parrish, D. F., and Derber, J. C.: The NMC method for estimating forecast error covariances using operational forecast data, Mon. Weather Rev., 120, 1747–1763, https://doi.org/10.1175/1520-0493(1992)120<1747:TNMCSS>2.0.CO;2 , 1992.

Poli, P., Healy, S. B., and Dee, D. P.: Assimilation of Global Positioning System radio occultation data in the ECMWF ERA-Interim reanalysis, Q. J. R. Meteorol. Soc., 136, 1972–1990, https://doi.org/10.1002/qj.722, 2010.

Purwar, S., Bankar, A., Rakesh, V., Choy, S., Li, H., Mohapatra, G., and Kuleshov, Y.: Impact of assimilating GNSS ground-based and space-based observations on extreme rainfall prediction over Karnataka, India, Int. J. Remote Sens., 46, 7780–7823, https://doi.org/10.1080/01431161.2025.2559423, 2025.

Prakash, S., and Srinivasan, J.: A comprehensive evaluation of near real-time and research products of IMERG precipitation over India for the southwest monsoon period, Remote Sens., 13, 3676, https://doi.org/10.3390/rs13183676, 2021.

ROM SAF: The Radio Occultation Processing Package (ROPP) Pre-processor Module User Guide, Tech. Rep. SAF/ROM/METO/UG/ROPP/004, Version 11.0, EUMETSAT ROM SAF, 2021.

Rodgers, C. D.: Inverse Methods for Atmospheric Sounding: Theory and Practice, World Scientific, Singapore, https://doi.org/10.1142/3171, 2000.

Schreiner, W. S., Weiss, J. P., Anthes, R. A., Braun, J., Chu, V., Fong, J., Hunt, D., Kuo, Y. H., Meehan, T., Serafino, W., Sjoberg, J., Sokolovskiy, S., Talaat, E., and Wee, T. K.: COSMIC-2 radio occultation constellation: First results, Geophys. Res. Lett., 47, e2019GL086841, https://doi.org/10.1029/2019GL086841, 2020.

Skamarock, W. C., et al.: A description of the Advanced Research WRF Version 4, NCAR Tech. Note, NCAR/TN-556+STR, https://doi.org/10.5065/1dfh-6p97, 2019.

Smith, E. K., and Weintraub, S.: The constants in the equation for atmospheric refractive index at radio frequencies, Proc. IRE, 41, 1035–1037, https://doi.org/10.1109/JRPROC.1953.274297, 1953.

Syndergaard, S.: Assessment of the structural uncertainty of GRAS products from level 1B (bending angles) up to level 2 (temperatures), Danish Meteorological Institute Technical Report under EUMETSAT Contract No. EUM/CO/10/4600:000745/AvE, 2012.

Tan, J., Petersen, W. A., Kirstetter, P. E., and Tian, Y.: Performance of IMERG as a function of spatiotemporal scale, J. Hydrometeorol., 18, 307–319, https://doi.org/10.1175/JHM-D-16-0174.1, 2017.

Xuan, Q. P., Chen, S.-Y., Huang, C.-Y., and Kuo, Y.-H.: Tropical cyclogenesis in the western North Pacific improved by GNSS RO data assimilation using hybrid 3DEnVar with a nonlocal excess phase operator, Weather Forecast., 40, 2255–2271, https://doi.org/10.1175/WAF-D-25-0010.1, 2025.

Zhang, H., Shao, H., Ruston, B., and Braun, J. J.: Impact study of increased radio occultation observations during the ROMEX period using JEDI and the GFS atmospheric model, Atmos. Meas. Tech., 18, 6167–6184, https://doi.org/10.5194/amt-18-6167-2025, 2025.

Zou, X., et al.: A ray-tracing operator and its adjoint for the use of GPS/MET refraction angle measurements, J. Geophys. Res., 104, 22301–22318, https://doi.org/10.1029/1999JD900450, 1999.